https://doi.org/10.1016/j.polymer.2021.123756

# Green preparation and enhanced gas barrier property of rubber nanocomposite film based on graphene oxide-induced chemical crosslinking

Linyan Wang[1, 2], JiangTao Zhang[1], Youyi Sun[1]*, Tao Zhang[1, 2], Long Wang[1], Jian Wang[1], Yurong Liang[1, 2], Mingzheng Hao[2], Qiang Fu[3]

1. School of materials science and technology, North University of China, Taiyuan 030051, PR China

2. Department of Materials Engineering, Taiyuan Institute of Technology, Taiyuan 030008, PR China

3. School of Civil and Environmental Engineering, University of Technology Sydney, Ultimo NSW 2007, Australia.

Abstract: A green and facile preparation method of graphene oxide/nitrile butadiene rubber (GO/NBR) nanocomposite film was developed for application in gas barrier. In the process, chemical crosslinks were formed by graphene oxide (GO)-induced crosslinking in absence of vulcanization ingredients. It was found that the GO-induced crosslinking occurred at a higher concentration of 1.0 wt% and a higher temperature of 170.0℃. The GO-induced crosslinking did not only enhance the crosslinking density of GO/NBR nanocomposite film, but also enhanced interfacial interactions between GO and NBR matrix. The resultant GO/NBR nanocomposites with 3.0wt% GO loading displayed enhanced tensile strength by ~145% as well as exhibited a dramatically decreased gas permeability coefficient by ~56% compared to the pristine NBR. The excellent comprehensive performance of GO/NBR nanocomposites was attributed to good barrier and high mechanical property of GO. In addition, the strong interfacial interaction between GO and NBR was also key role for enhancing tensile strength and barrier of GO/NBR nanocomposites. This ‘green’ and facile method provides new insights for the fabrication of high-performance GO/rubber composites for various applications.

Keywords: Graphene oxide; Nitrile rubber latex; Segregated structure; Self-crosslinking; Gas barrier property

Responding author: Fax: 86-351-3559669

E-mail address: syyi@pku.edu.cn (YY. Sun)

## 1.Introduction

Rubber barrier materials are widely used in aerospace, tire inner liners, food and drug packaging, personal protective equipment and other barrier application due to their advantages, such as multi-functions, lightweight, ease of processing, low-cost, high elasticity and recovery from deformation [1]. However, the pure rubbers usually displayed insufficient gas barrier properties, which limits their applications under certain special conditions, such as current aerospace, tire inner liners and vacuum-insulating applications [2]. Various strategies including layer-by-layer assembly [3], dynamic vulcanization [4], surface coating [5] and incorporation of impermeable two-dimensional (2D) fillers (e.g. organic clay [6], boron nitride [7], graphene [8]and graphene oxide (GO) [9], etc) have been developed to improve the gas barrier properties of rubbers. Among these methods, introduction of GO into the rubber matrix has been one of the simplest and most effective methods [10-12]. The improvement of the gas barrier properties is attributed to the tortuous diffusion path of the gas molecules created by the impermeable GOs toward He (0.26 nm), $H_2$ (0.289 nm), $O_2$ (0.346 nm), $N_2$ (0.364 nm) and other gases [13-14]. In addition, GOs contains various hydrophilic groups, including epoxide, hydroxyl and carboxyl groups, which enables GOs to have a good interfacial interaction with polar polymers and thereby facilitates the load transfer between GO and polymer matrix [15]. Previous works have revealed that the gas barrier property of such GO/rubber composites was effectively improved and strongly dependent on the fraction [16-17], the aspect ratio [18-19], dispersion [20-21] and the orientation or distribution of GOs [22-23]. For example, for GO/natural rubber (NR) composites, increasing the fraction of GO nanosheets from 0 to 1.0 wt% can result in a 55% reduction in air permeability [16]. While increasing the aspect ratio of GO nanosheets from 97 to 226 at the same GOs loading caused a 38% reduction in oxygen ($O_2$) permeability [18]. Promoting the dispersion of GOs in fluoroelastomer (FKM) via hydrogen bond can reduce $O_2$ permeability by 32% compared with the control sample with poor GOs dispersibility [20]. Compared with non-segregated orientation counterpart, the GO/butadiene styrene rubber (SBR) composites with segregated orientation (1.66 vol%) displayed an enhanced gas barrier property [22]. In addition to the above factors, the interfacial interaction between GOs and rubber also plays a crucial role in restricting rubber chain mobility, reducing interfacial voids, and thereby

improving the gas barrier properties [24]. In order to enhance interfacial interaction between GOs and rubbers, chemists and/or engineers have modified the surface of GOs by introducing functional groups that can interact with the rubber chains, such as bis(triethoxysilylpropyl)-tetrasulfide (BTESPT) [16], α-bromoisobutyryl bromide [11] and sulfur [25]. Although synthesis and gas barrier properties of GO/rubber nanocomposites have been reported, yet these GO/rubber nanocomposites were based on chemical vulcanization crosslinking and there were lots of vulcanization ingredients to be used. It did not only affect the dispersion and network formation of GO in rubber matrix, but also it was not environment friendly. In addition, the surface modification process was complicated and consumed many organic solvents, which limits its practical applications. Therefore, up to now, it is still interesting to find a green and facile method of preparing GO/rubber composites with high performance for various applications. Recently, unlike conventional inert fillers and surface-treated nanoparticles, GO can not only act as fillers, but also can generate free radicals by thermal treatment, initiating polymerization on surface of GO [26~27]. From this respect, the GO/rubber composite maybe prepared by GO-induced crosslinking method, which can effectively avoid to use vulcanization ingredients and complicate surface modification. In addition, NBR rubber has found widespread use in the automotive (seals, hoses, and bearing pads), petroleum (stators, well head seals, and valve plates), electrical (cable sheathing), shipbuilding (pipe seals and couplings) industries and so on due to excellent physical and chemical properties [28-29]. However, up to now, GO-induced crosslinking of GO/rubber composites is few reported to enhance gas barrier of GO/rubber composites, especially for segregated GO/nitrile rubber latex (NBR) nanocomposites.

In this work, a novel method was developed to facile and green preparation of GO/NBR nanocomposites, in which free radicals were generated on surface of GO at high temperature and then induced the chemical crosslinking of NBR in absence of vulcanization systems. The effects of GO content and temperature on GO-induced crosslinking process were investigated in detail. As expected, the self-crosslinking leaded to strong interfacial interactions and efficient load transfer between GO sheets and NBR matrix. Furthermore, the GO/NBR nanocomposites with segregated structure were constructed by the self-assembly latex method. The resultant GO/NBR nanocomposites

with 3.0wt% GO loading exhibited a dramatically decreased gas permeability coefficient by ~56%. This water-mediated, environmentally friendly and 'green' method is suitable to produce high-performance GO/rubber composites for various applications.

## 2.Experimental

### 2.1Materials

Graphene oxide (GO) aqueous solution (2mg/mL) was purchased from Tang Shan Jianhua Graphene Technology Co. Ltd. Polyvinyl pyrrolidone (PVP, MW=10 kDa, K=13~18) was purchased from Aladdin reagent Co. Ltd. Nitrile rubber latex (NBR, 43.5 wt.% of NBR content, FSDJ52) was supplied by Lao chemical Co. Ltd.

### 2.2 Preparation of GO/NBR nanocomposites

The segregated GO/NBR nanocomposites was prepared by combing self-assembled latex with GOs induced crosslinking as shown in following. The PVP modified GOs were firstly synthesized according to previous work [30]. Specifically, PVP was added to a GOs suspension (2 mg/mL) under ultrasonic treatment for 5 h to obtain a stable aqueous suspension of PVP@GOs with a PVP/GO wight ratio of 1:1. Subsequently, the PVP@GOs suspension was added to NBR latex solution to form an aqueous suspension under mechanical agitation for 1 h at room temperature. Then the aqueous suspension was dried at 60℃ for 24h to obtain the GO/NBR nanocomposites. Finally, the GO/NBR nanocomposites were further thermally vulcanized at a certain temperature (160℃, 170℃, 180℃, 190℃ and 200℃) for 105 min to obtain different crosslinking densities. For a comparison, the GO/NBR nanocomposites with various GOs loads (0, 0.5wt%, 1.0wt%, 2.0wt%, 3.0wt% and 5.0wt%) were prepared by adjusting the volume of PVP@GO suspension. These nanocomposites are abbreviated as x% GO/NBR, where x denotes the PVP@GO content in the nanocomposites.

### 2.3 Characterizations

Wide angle X-ray diffraction (WAXD) was performed on Rigaku Smartlab. Scanning was at a speed of 5°/min, from 3° to 60°.

Raman spectra were recorded from 100 to 4000 $cm^{-1}$ on an IRKT46 (Reniseau, UK) and the wavelength of the laser used was 532.0nm.

The ultra-thin transmission electron microscopy (TEM) sample was cut using a cryogenic ultramicrotome Leica ultracut EM UC6 (Germany) at -60℃ and

micro-structure of GO/NBR nanocomposites was observed by Tecnai 12(Philips Netherlands).

The crosslinking process was analysed with an oscillating disc rheometer (ODR, M3000-A, Gotech Testing Machines Inc, Taiwan). After pre-heating the discs of ODR to a programmed temperature, 4.0g GO/NBR composites were inserted between the two discs and the torque was monitored as a function of time.

Fourier transform infrared (FTIR) measurements were carried on a Bruker Tensor 27 spectrometer with KBr thin pellets in the wavenumber range of 4000-400 $cm^{-1}$.

X-ray photoelectron spectroscopy (XPS) was performed on a ThermoFischer, ESCALAB 250Xi (USA) with Al Kα radiation of 1486.6 eV.

Electron spin resonance (ESR) measurements were carried out on a Bruker EMXplus instrument at 180℃ under different time, the power and frequency of the microwave radiation were 1.0 mW and 9.4 GHz, respectively.

The equilibrium swelling ration (ESR) and crosslinking density were determined by equilibrium swelling measurements. A piece of GO/NBR composites, approximately 10 mm×5mm, was immersed in toluene for a week to extract the sol fraction, during which the solvent bath was replaced with fresh toluene every day.

The ESR was obtained according to following equation.

$$ESR = \frac{W1}{W2} \qquad (1)$$

Where, $w_1$ is the weight of rubber and solvent in the swollen sample and $w_2$ is the weight of rubber in the deswollen rubber.

Crosslinking density was determined according to Flory-Rehner equation [31-32]:

$$Ve = -\frac{\ln(1-V_r)+V_r+\chi V_r^2}{V_s\left(V_r^{1/3}-V_r/2\right)} \qquad (2)$$

Where $\nu_r$ is the volume fraction of the crosslinked polymer swollen to equilibrium and $\nu_s$ is the solvent molar volume (106.2 $cm^3$/mol for toluene). $\chi$ is the NBR-toluene interaction parameter and is taken as 0.435.

$$Vr = \frac{W_4/\rho_2}{W_4/\rho_2+(W_3-W_4)/\rho_1} \qquad (3)$$

Where $w_3$ is the weight of the swollen gel, $w_4$ is the weight of the gel after drying, $\rho_1$ and $\rho_2$ are the densities of the solvent and the NBR and are taken as 0.866g/mL and 1.0g/ $cm^3$, respectively.

Nuclear magnetic resonance spectroscopy (NMR) was performed on VTMR20-010V-1 (Suzhou NIUMAG) at 90℃, the frequency used by the sensor was 200KHz.

Dynamic-mechanical analysis (DMA) measurements were conducted on a Q800 (TA, USA) in the tension mode at a frequency of 1 Hz in the range of -60℃~ 40℃ at a heating rate of 3℃/min.

The strain amplitude dependence of storage modulus was measured on an elite RPE2-0026 rubber processing analyser (TA, USA) at 60℃, 0.1Hz and the amplitude from 1 to 1200%.

Tensile tests were performed using GOTECH AI-7000M instrument (Gotech Testing Machines Inc, Taiwan) at room temperature following GB/T 528-2009. The crosshead speed was 500mm/min. The dumbbell shape samples were 75mm in length, 1mm in thickness and 4mm in width. The reported values were the average of three measurements. Shore A hardness was performed following GB/T 531-2008 using GS-701N instrument (Gotech Testing Machines Inc, Taiwan) and the reported values were the average of three measurements.

The morphologies of the freeze-fractured surfaces of the GO/NBR composites were taken with the scanning electron microscope (SEM, JSM-7200F, Nippon Electronics co. LTD), at an acceleration voltage of 10.0kV with gold coating. The gold was coated on surface of samples before measurement.

Nitrogen permeability of GO/NBR composites (70.0mm in diameter) were tested at 23 and 40 C using a Gas Permeability Tester (GPT200, RADE, Beijing, China).

## 3. Results and discussion

### 3.1 Preparation of segregated GO/NBR nanocomposites

Here, a new facile and green process was developed to prepare GO/NBR nanocomposite film with segregated structure in absence of additives as shown in Scheme 1A. In water evaporation stage, the GO/NBR composite particles move about freely with their Brownian motion, forms irreversible contact and ends with their coalescence to form

a continuous film with segregated network structure. In crosslinking stage, NBR molecules across the ruptured shell of GO, and then diffuse, permeate and entangle each other, forming a physical crosslinking [33-34]. In addition, the peroxide groups on GO nanosheets can generate two types of radicals (i.e. hydroxyl radicals on cleaved groups and free radicals on GO) at high temperature as shown in Scheme 1B. The generated hydroxyl radicals can diffuse into the rubber matrix, leading to chemical crosslinking of the rubber chains, meanwhile the carboxyl radicals and free radicals on surface of GO nanosheets can cause chemical crosslinking between GO and rubber chains [26]. Thereby, in the process, it does not only form segregated network structure with self-crosslinking for GO/NBR composites, but also it is green or environment friendly.

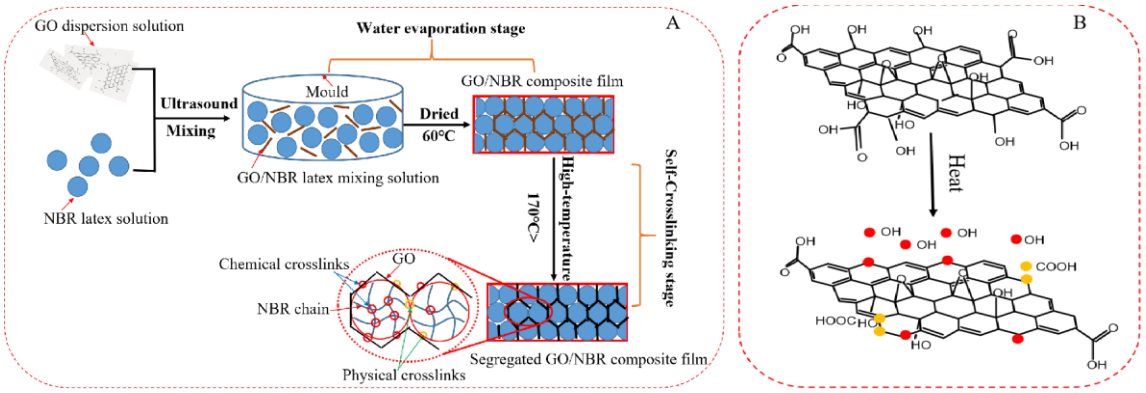


Scheme 1. (A)The preparation process and (B) self-crosslinking mechanism of GO/NBR nanocomposites.

The XRD patterns of GO, NBR and GO/NBR nanocomposites (3.0wt%) without and with thermal treatment were firstly characterized and compared as shown in Fig.1A. It clearly showed a sharp characteristic peak at 2θ=11.4° for GO sample, corresponding to the (002) reflection of GO. The peak at 2θ=11.4° corresponded to an interlayer spacing of 0.79nm, resulting from the accommodation of various oxygen-containing groups [35]. For the pure NBR and GO/NBR nanocomposite, they both showed a similar broad peak at 2θ=18.7°, which was assigned to the amorphous NBR. However, the characteristic peak assigned to GO was not observed for GO/NBR nanocomposite. The result indicated that GO nanosheets were finely dispersed in NBR matrix without any re-stacked aggregates [36]. In addition, it was found that the XRD patterns of GO/NBR nanocomposite with and without thermal treatment showed similar curves. The result indicated that the effect of thermal treatment on dispersion and reduction degree of GO in

NBR matrix was slight. Furthermore, the XRD patterns of GO/NBR nanocomposite with and without thermal treatment were also characterized and compared as a function of GO content as shown in sFig.1. All samples showed similar curves, in which the peak assigned to GO was not observed. The result suggested the good dispersion and few re-stacked aggregates of GO in NBR matrix for various GO contents. In addition, the XRD peak' intensity of GO/NBR nanocomposite was slight change as a function of GO content due to the relatively low content. The successful preparation and micro-structure of GO/NBR nanocomposites was further confirmed by Raman spectra as shown in Fig.1B. All profiles showed two similar peaks at 1341 and 1570 $cm^{-1}$, which were assigned to D and G bands of GOs [37]. In addition, the G peak of GO blue shifted from 1576 to 1570 $cm^{-1}$, which was attributable to the loss of $sp^2$ orbitals and the formation of defects on GO nanosheets due to the extensive oxidation [38]. These results confirmed the presence of GO in NBR matrix after the thermal self-crosslinking. In a comparison, the $I_D/I_G$ values are 0.95, 1.08 and 1.29 for pristine GOs, 3 wt% uncross-linked and crosslinked GO/NBR nanocomposites, respectively. The peak intensity ratio $(I_D/I_G)$ increased following this order: GO<uncross-linked< crosslinked GO/NBR nanocomposites. The increased D peak intensity of (un)cross-linked GO/NBR nanocomposites can be attributed to the surface-grafting rubber chains, which can prevent the agglomeration of the GO sheets. This result also indicated the formation of crosslinked NBR on the surface of GOs. The dispersion and distribution of GO in NBR matrix were characterized by TEM measurements and the images are shown in Fig.1C and D. It can be clearly seen that single layer or a few stacked layers of GOs were uniformly dispersed in the NBR matrix and had a segregated network morphology, in which the submicro NBR latex particles were covered by GO nanosheets through the self-assembly process.

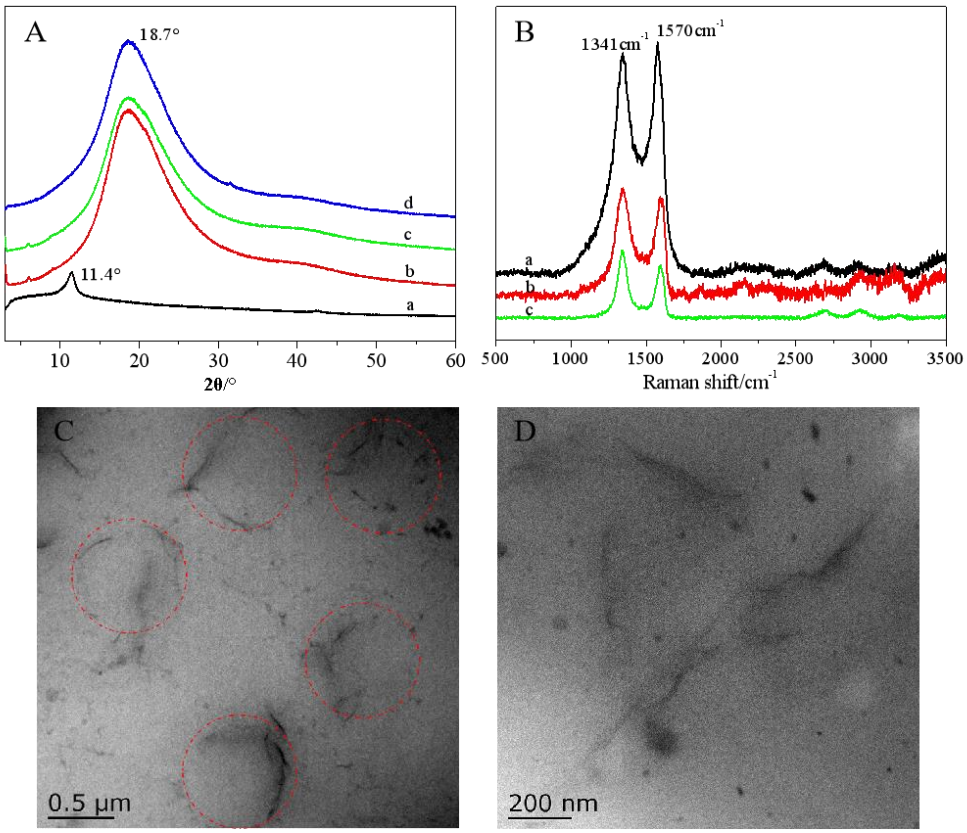


Fig.1. (A) XRD patterns of (a) GO, (b) NBR, GO/NBR nanocomposites (c)without ad (d)with thermal treatment. (B) Raman spectra of (a) GO, GO/NBR nanocomposites (b)without ad (c)with thermal treatment. (C-D) TEM images of GO/NBR nanocomposites with thermal treatment.

GO-induced crosslinking of GO/NBR nanocomposites was firstly investigated as a function of treatment temperature or GO content by oscillating disc rheometer (ODR) as shown in sFig.2. The vulcanization parameters were displayed in sTable.1 according to the curing curves. It was found that there was a smaller torque ($M_L$) and a larger torque ($M_H$) at a higher GO content (Fig.2A-B), which was attributed to the improved dispersion of GO nanosheets and the strong interfacial interactions between GO nanosheets and NBR. Here, ΔS was also calculated from torque ($M_L$) and torque ($M_H$) and correlated with the crosslinking density. Specifically, the larger ΔS indicated a higher crosslinking density [39]. As shown in Fig.2C, when the treatment temperature increased, the ΔS values of pure NBR and GO/NBR nanocomposites with 0.5 wt% and 1.0 wt% GO content remained the same; while the ΔS values of GO/NBR nanocomposites with a

higher GO content (*i.e.* 2.0 wt% or 3.0 wt%) increased sharply. The result indicated that when the GO content exceeded 1.0 wt%, GO-induced crosslinking occurred in the GO/NBR nanocomposites at high temperature. The curves d and e shown in Fig.2C also indicated that the self-crosslinking reaction was temperature-dependent. As expected, these results indicated that the self-crosslinking of GO/NBR nanocomposites strongly depended on GO content and treatment temperature.

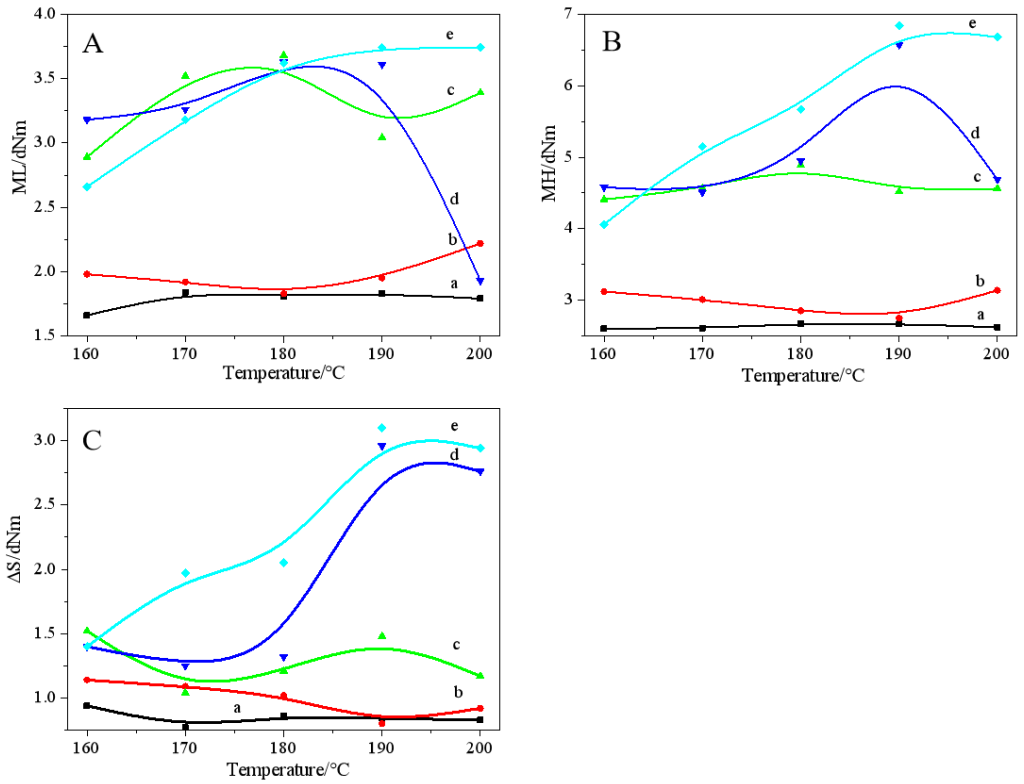


Fig.2. (A) $M_L$, (B) $M_H$ and (C) ΔS of GO/NBR nanocomposites with various GO contents of (a) 0, (a)0.5wt%, (a)1.0wt%, (a)2.0wt% and 3.0wt% as a function of treatment temperature.

The GO-induced crosslinking of GO/NBR nanocomposites was further measured and confirmed by the FT-IR spectra as shown in Fig.3. For pure GO, the peaks at 3425$cm^{-1}$, 1736$cm^{-1}$,1628$cm^{-1}$, 1179$cm^{-1}$ and 1098$cm^{-1}$ were assigned to the vibration of hydroxyl groups, the C=O stretching vibration, the C=C stretching vibration, C-OH telescopic vibration and the C-O-C vibration, respectively as shown in Fig.3A[40]. For pure NBR, the peaks at 2237$cm^{-1}$ and 1638$cm^{-1}$ were assigned to the C≡N groups and C=C bonds of NBR (in Fig.3B) [41]. As shown in Fig.3C, lots of peaks assigned to GO

and NBR were almost observed in the GO/NBR nanocomposite without thermal treatment. In addition, the peaks at 3425cm$^{-1}$ and 1652cm$^{-1}$ assigned to the vibration of hydroxyl groups and C=C bonds of NBR increased dramatically. The result was attributed to entanglement of NBR chains, indicating the formation of physical crosslinking. When the GO/NBR nanocomposites were thermally treated, the peaks at 2237cm$^{-1}$ and 1652cm$^{-1}$ shifted and became weaker as shown in Fig.3D. The result was attributed to GO-induced crosslinking of C≡N groups and C=C bonds in NBR. Above result was further confirmed by the FT-IR spectrum as shown in Fig.3E. It clearly showed FT-IR spectrum of GO after heat treatment at 180°C for 105 min. The oxygen-containing functional groups of hydroxyl groups, C-OH telescopic vibration and the C-O-C vibration loss its intensity and the peak area reduced dramatically, indicating that the bond breakage of oxygen-containing functional groups of GO [18]. These results indicated the formation of crosslinked NBR on the surface of GO by GO-induced crosslinking method.

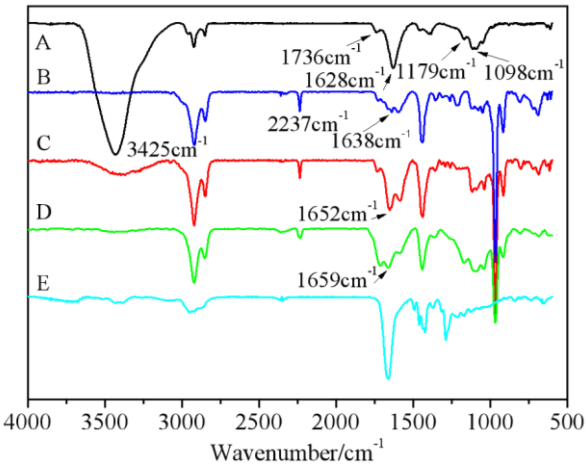


Fig.3. FT-IR spectra of GO (A) without and (E) with high temperature treatment, (B)NBR, GO/NBR nanocomposite (C) without and (D) with high temperature treatment.

To confirm the GO-induced crosslinking, the GO nanosheets before and after thermal treatment were characterized by XPS measurements and the results were shown in Fig.4A-C. The C1s spectrum of GO was deconvoluted into four peaks with binding energy of 284.8, 286.5, 287.0 and 288.5 eV, corresponding to C-C/C=C, C-O, C=O and O-C=O, respectively as shown in Fig.4B [42-43]. After thermal treatment at 180°C for 1

h, the peak intensity of C-O and C=O significantly decreased (Fig.4C) and the C/O ratio increased from 2.45 to 3.29 (Fig.4A survey scan). These results confirmed the bond breakage of C-OH and C-COOH bonds [26]. Since the electron spin resonance (ESR) intensity was proportional to the concentration of radicals, the GO nanosheets were further characterized by ESR spectra to provide direct evidence for the generation of hydroxyl radicals at high temperature. As shown in Fig.4D, the signal intensity obviously increased with the extension of heating time, which indicated continuous production of radicals due to the cleavage of oxygenic groups on GO nanosheets.

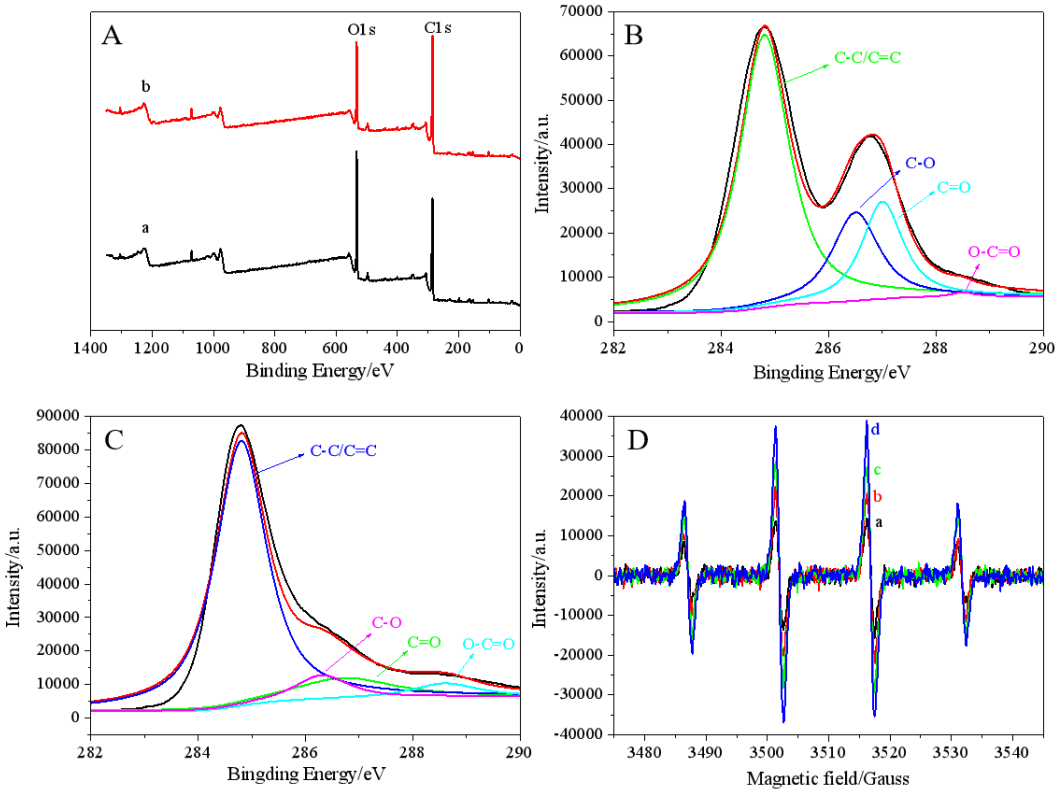


Fig.4. (A) XPS spectra of the survey scan, GO (a) without and (b) with thermal treatment. The C1s of GO without (B) before and (C) with thermal treatment, (D) ESR spectra of $OH^{\cdot}$ of GO with thermal treatment at 180 ℃ for various times of (a) 4min, (b) 8min, (c)12min and (d) 20min.

GO-induced crosslinking of GO/NBR nanocomposites was further characterized and confirmed by equilibrium swelling method. As shown in Fig.5A and B, the equilibrium swelling ratio (ESR) and the crosslinking density of the GO/NBR nanocomposites with and without thermal treatment remained the same when the GO content was increased. In

contrast, the ESR of GO/NBR nanocomposites decreased with the increase of GO content after thermal treatment (Fig.5A), which was attributed to the high crosslinking density caused by the high GO content as aforementioned above. Subsequently, the crosslinking density of the GO/NBR nanocomposites was calculated quantitatively through the equilibrium swelling method. As shown in Fig.5B, after thermal treatment, the crosslinking densities of the pristine NBR and the GO/NBR nanocomposites with3.0wt% GO content were 0.145 and 2.45 mmol/cm$^3$, respectively. In addition, we also found that the crosslinking density increased rapidly when the GO content exceeded 1.0 wt%, which again showed that 1.0wt% was the critical GO content for GO -induced crosslinking of NBR. We further performed Nuclear magnetic resonance (NMR) spectroscopy characterization on these samples to evaluate above results (sFig.3). As shown in Fig.5C, both the chemical and total crosslinking density of GO/NBR nanocomposites calculated by NMR increased with the increase of GO content, agreeing well with above results obtained from equilibrium swelling method. While the physical crosslinking due to entanglement between rubber macromolecular chains was independent from GO content. This result clearly showed that the GO-induced crosslinking was an irreversible chemical reaction. We further characterized the relaxation time ($T_2$) of GO/NBR nanocomposites after thermal treatment, corresponding to the mobility of the cross-linked network. As shown in Fig.5D, the crosslinked GO/NBR nanocomposites displayed a decreased $T_2$ value with increasing in the GO content, which indicated an increase in cross-linking density [44-45]. As expected, the $T_2$ values of GO/NBR nanocomposites without thermal treatment remained the same when the GO content increased. In summary, all these results confirmed the formation of chemically cross-linked GO/NBR nanocomposites (induced by GO) after thermal treatment.

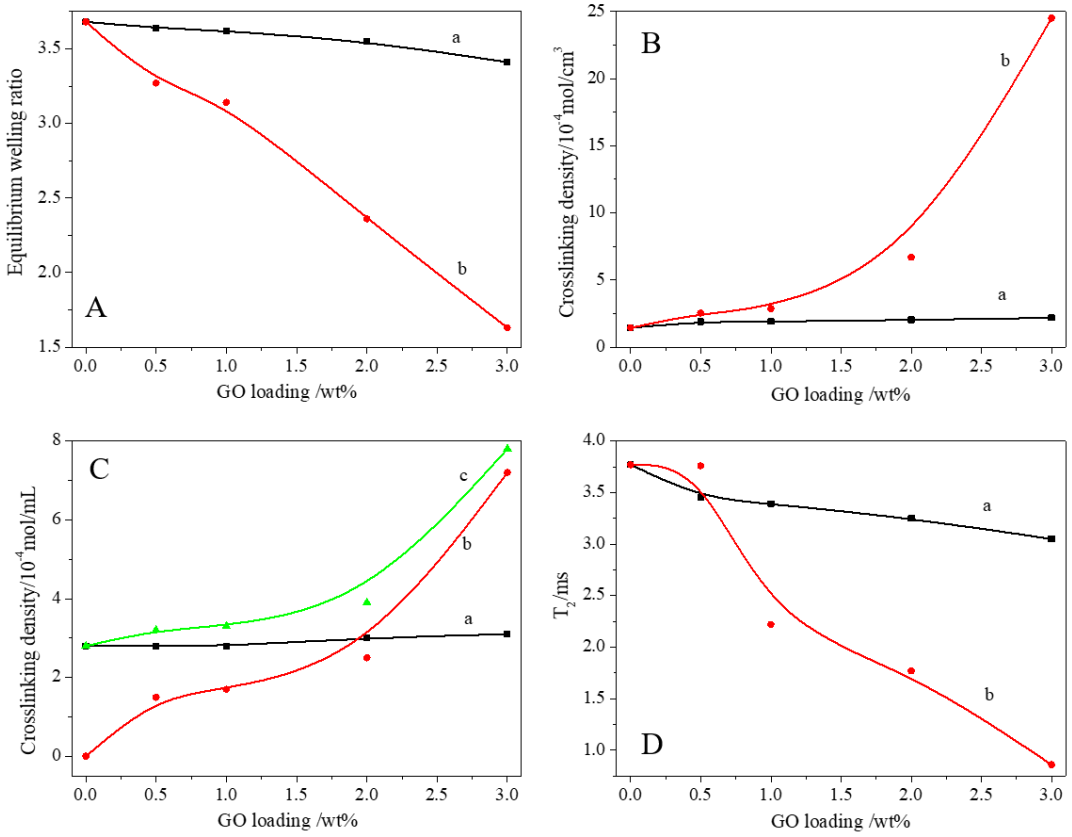


Fig.5. (A) Equilibrium swelling ratio and (B) crosslinking density of GO/NBR nanocomposites (a)without and (b)with thermal treatment as a function of GO content by equilibrium swelling method. (C) The crosslinking density of GO/NBR nanocomposites with thermal treatment as a function of GO content by NMR method: (a) physical, (b) chemical and (c) total crosslinking density. (D) The relaxation time ($T_2$) of GO/NBR nanocomposites (a)without and (b) with thermal treatment as a function of GO content by NMR method.

3.2 Mechanical properties of segregated GO/NBR nanocomposites

The dynamic mechanical performance was firstly characterized to evaluate the interfacial interactions between GO nanosheets and NBR chains by DMA method as shown in Fig.6. It clearly Fig.6 showed the storage modulus (*G'*) and the tan delta (*tanδ*) as a function of treatment temperature, and the detailed results were listed in Table1. Regardless of before and after thermal treatment, the G' and glass transition temperature ($T_g$) of the GO/NBR nanocomposites increased with the increase of GO content. The result indicated a significant decrease in mobility of NBR chain around GO nanosheets

due to the crosslinking as well as an efficient load transfer from the rubber chain to GO nanosheets [46]. In a comparison, the GO/NBR nanocomposites with thermal treatment displayed a larger $G'$ or $T_g$ compared to the composites without thermal treatment and other rubber composites reported in previous works [47]. The result was mainly attributed to strong interfacial interactions between GO and NBR, resulting from GO-induced crosslinking between GO and NBR chains. In addition, graphene with high Young's modulus of 1.0 TPa was also key role for the large storage modulus. Compared to the pristine NBR, the $T_g$ of GO/NBR nanocomposites with wt% and 3.0wt% GO content was improved to be 6.0℃ or 11.0℃, respectively. This result further confirmed that higher GO content led to higher crosslinking density and stronger interfacial interactions.

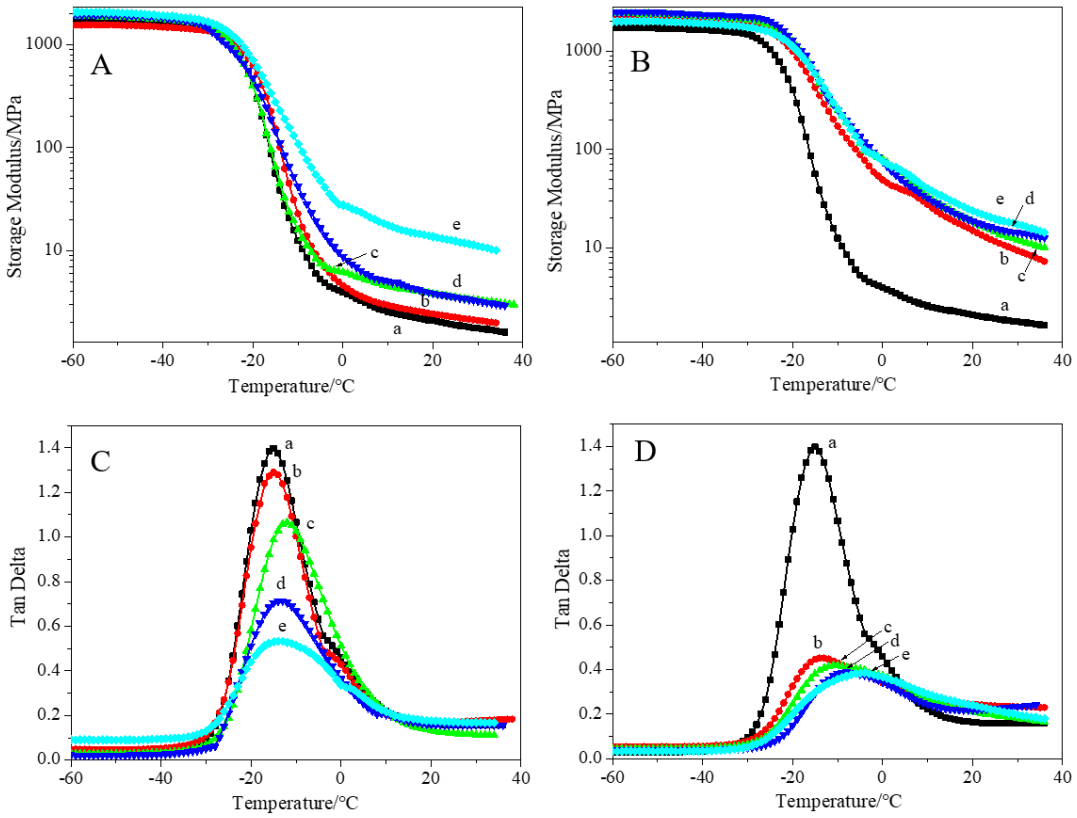


Fig.6. Storage modulus vs temperature of GO/NBR nanocomposites (A) without and (B) with thermal treatment as a function of GO content. Tan delta vs temperature of GO/NBR nanocomposites (C) without and (D) with thermal treatment as a function of GO content, (a) 0, (b) 0.5wt%, (c) 1.0wt%, (d) 2.0wt% and (e) 3.0wt%.

Table 1. The parameters GO/NBR nanocomposites determined from the DMA curves

| Materials | NBR | GO/NBR without treatment | | | | GO/NBR with treatment | | | |
|---|---|---|---|---|---|---|---|---|---|
| Content(wt%) | 0 | 0.5% | 1.0% | 2.0% | 3.0% | 0.5% | 1.0% | 2.0% | 3.0% |
| Tg (℃) | -15.0 | -15.0 | -12.8 | -13.1 | -13.0 | -13.9 | -11.0 | -8.7 | -4.1 |
| tanδ peak | 1.40 | 1.29 | 1.06 | 0.71 | 0.53 | 0.45 | 0.42 | 0.39 | 0.38 |

The effect of the strain amplitude on the storage modulus (G') of GO/NBR nanocomposites without and with thermal treatment was also investigated and compared as shown in Fig.7. The *G*' of all samples almost remained the same at low strain region and then dramatically deceased when the strain was further improved to be larger than 30%. The result was attributed to Payne effect [48]. The Payne effect described the breakdown of physical filler networks when oscillatory shear was applied, which was caused by filler-filler interactions and filler-rubber interactions [48-49]. In addition, at the low strain region, the *G*' increased with the increase of GO content, indicating that the GO-rubber interactions as well as the Payne effect were both enhanced [49]. This result again showed that the crosslinking density of the networks increased with increasing in GO content.

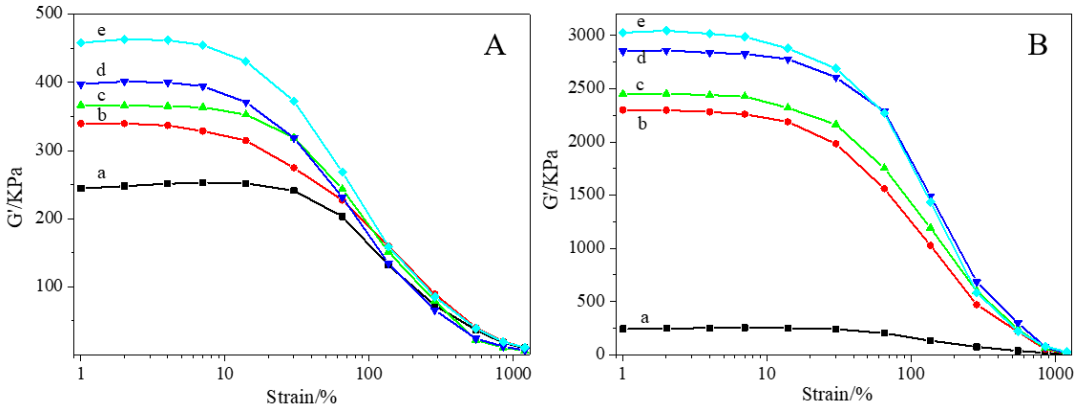


Fig.7. The *G*' *vs.* strain curves of GO/NBR nanocomposites (A) without and (B) with thermal treatment with various GO contents of (a) 0, (b) 0.5wt%, (c) 1.0wt%, (d) 2.0wt%, and (e) 3.0wt%.

Tensile mechanical properties of GO/NBR nanocomposites without and with thermal treatment were investigated as shown in Fig.8A and 8B, respectively. The tensile strength firstly increased and then decreased with increasing in GO content for GO/NBR

nanocomposites without and with thermal treatment. GO/NBR nanocomposites without and with thermal treatment showed largest tensile strength of 0.8MPa and 3.23MPa for the 2.0wt% and 3.0wt% GO content, respectively. The result was attributed to mechanical reinforcing effect of GO and strong interfacial interaction between the GO and NBR matrix. When the content of GO was improved to be 5.0wt%, there was more restacked GO nanosheets and poor dispersion of GO in NBR matrix, leading to a decrease of tensile strength. In addition, it was found that the elongation at break of GO/NBR nanocomposites without and with thermal treatment both decreased with increasing in GO content. Especially, the GO/NBR nanocomposites almost lost plastic or elastic deformation at higher GO content than 3.0wt%. These results were attributed to that GO-induced crosslinking also increased the rigidity of GO/NBR nanocomposites by restricting the mobility of the NBR chains, and thereby reduced their elongation at break [50-51]. In a comparison, tensile strength (3.23MPa) of GO/NBR nanocomposites with thermal treatment was almost three times than (0.8MPa) that of GO/NBR nanocomposites without thermal treatment. The result was attributed to GO-induced crosslinking of GO/NBR nanocomposites with thermal treatment. When the matrix bears external load, the stress will be transferred through the interfacial connections, and the main load will be borne by the fillers, thus giving the composite materials excellent mechanical properties [50]. As shown in Fig.8C, we observed similar trend for Shore A hardness of GO/NBR nanocomposites without and with thermal treatment as a function of GO content. Specifically, the shore A hardness of GO/NBR nanocomposites without and with thermal treatment both increased monotonically with increasing in GO content. Furthermore, the GO/NBR nanocomposites with thermal treatment displayed a higher shore A hardness compared to their counterparts without thermal treatment. These results were also mechanical reinforcing effect of GO and strong interfacial interaction between the GO and NBR matrix. Above result were further confirmed by the SEM images of fracture surface of GO/NBR nanocomposites as shown in sFig.5. GO nanosheets restacked on the tensile fracture surface of GO/NBR nanocomposites without thermal treatment, indicating the poor adhesion between the GO nanosheets and NBR matrix due to no crosslinking. After thermal treatment, GO/NBR nanocomposites showed a smoother tensile fracture surface, indicating that the crosslinking enhanced the interfacial

connection between GO and rubber matrix, so no fracture failures occurred in the interfacial area. These results further confirmed that GO-induced crosslinking effectively improved the interfacial interaction between GO nanosheets and rubber matrix, thereby significantly improving the mechanical strength.

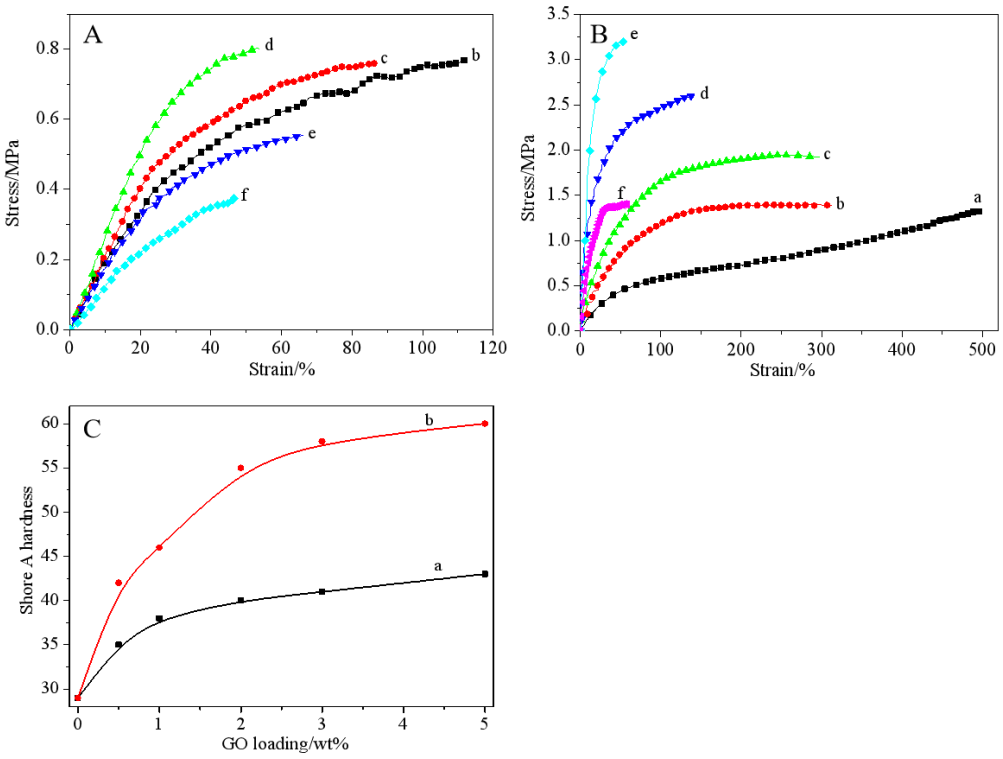


Fig.8. Stress-strain curves of GO/NBR nanocomposites (A) without and (B) with thermal treatment as a function of GO content (a) 0, (b) 0.5 wt%, (c) 1.0 wt%, (d) 2.0 wt%, (e)3.0 wt% and (f) 5.0wt%, respectively. (C) Shore A hardness of GO/NBR nanocomposites (a) without and (b) with thermal treatment as a function of GO content.

3.3 Gas barrier property of segregated GO/NBR nanocomposites

Gas barrier properties of the present GO/NBR nanocomposites without and with thermal treatment were investigated and compared as a function of GO content as shown in Fig.9A. It clearly showed that the $N_2$ permeability of all nanocomposites progressively decreased with increasing in GO content. The result was attributed to good barrier properties of incorporated GO nanosheets by creating a tortuous diffusion path in the matrix (lower permeability suggests better gas barrier property). In a comparison, the

GO/NBR nanocomposites with thermal treatment showed lower permeability compared with the GO/NBR nanocomposites without thermal treatment at the same GO content. For example, the permeability coefficient of untreated GO/NBR nanocomposites (3.0wt%) was about $5.65\times10^{-17}m^2s^{-1}Pa^{-1}$, while the permeability coefficient of treated GO/NBR nanocomposites (3.0wt%) dramatically decreased to $4.14\times10^{-17}m^2s^{-1}Pa^{-1}$. This value was only 44% of the pristine NBR permeability. When the GO content was further improved to 5.0wt%, the permeability coefficient of untreated and treated GO/NBR nanocomposites both showed slight change to $5.31\times10^{-17}m^2s^{-1}Pa^{-1}$ and $3.82\times10^{-17}m^2s^{-1}Pa^{-1}$ compared to GO/NBR nanocomposites with 3.0wt% GO content, respectively. It is well known that the temperature can affect gas permeability [17]. Usually, when rising temperature, gas diffusivity and materials free volume both increased, leading to an increase in gas permeability [52-53]. Interestingly, in this study, we observed that the permeability coefficient of GO/NBR nanocomposites at 23℃ was almost identical to that at 40℃, especially at high GO content (Fig.9A). This result might be attributed to the enhancement of interfacial interaction after thermal treatment, thereby suppressing the increase in free volume caused by temperature. According to the modified Nielson model [54], we modelled the dependence of the relative gas permeability on the GO volume fraction ($\Phi_f$) and its aspect ratio(2r/d) by using eq. (4)

$$\frac{P}{P_0} = \frac{1-\Phi f}{1+(\frac{r}{d})(\frac{\Phi f}{3})} \quad (4)$$

Where $P$ and $P_0$ are the permeability coefficient of GO/NBR nanocomposites and pure NBR, respectively.

Fig.9B shows the relative $N_2$ nitrogen permeability coefficient ($P/P_0$) of the nanocomposites as a function of the GO volume fraction. $P/P_0$ dramatically decreased with increasing in GO volume fraction. The curve fitted with eq. (4) showed a r/d value of 243, indicating that the average aspect ratio (2r/d) of the GO nanosheets was about 486. This value agrees well with previously reported results, such as GO/XNBR [15], EG/ACM [55], and EG/XNBR [56] (Table 2). Such a high aspect ratio also suggested good dispersion of GO in the NBR matrix. The gas barrier and mechanical property of the present nanocomposites were compared with other rubber composites based on GO or rGO reported in previous works [15, 24, 28, 55-60] as shown in Table 2 and sTable 2, respectively. As listed in the Table 2, the present treated GO/NBR nanocomposites had

the lowest GO content (1.39vol%) in absence of vulcanization ingredients, but they still displayed outstanding gas barrier property with high relative reduction of 56.0%. In addition, although present GO/NBR nanocomposite was prepared in absence of vulcanization ingredients, it still showed similar mechanical properties with other GO/NBR nanocomposites prepared in presence of chemical vulcanization ingredients [59-60]. At the same time, highest enhancing rate of tensile strength was obtained for present GO/NBR nanocomposite. These results were attributed to that GO-induced crosslinking and segregated structure of GO in NBR matrix, leading to an improvement of gas barrier and mechanical property [61].

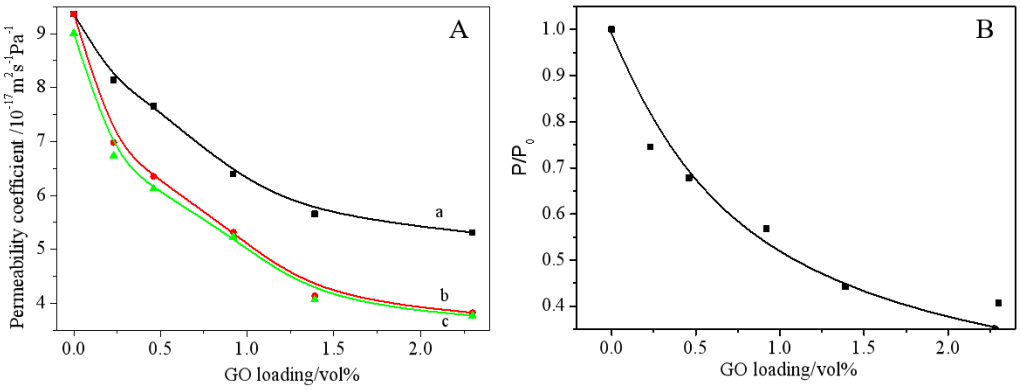


Fig.9. (A) Nitrogen permeability vs GO content curves of GO/NBR nanocomposites (a) without thermal treatment at 40℃, with thermal treatment at (b)40℃ and (c) 23℃. (B)The relative permeability of GO/NBR nanocomposites with thermal treatment as a function of GO at 40℃.

Table 2. Gas permeability and the aspect ratio of rubber composites based on GO or rGO.

| Rubber | Filler | Content | Processing | Permeant | Relative reduction(%) | The aspect ratio |
|---|---|---|---|---|---|---|
| XNBR[15] | GO | 1.9vol% | Latex | Nitrogen | 55 | 450 |
| VPR[24] | GO | 3.6vol% | Latex | Nitrogen | 40 | — |
| ACM[55] | EG | 9.1wt% | Latex | Nitrogen | 57 | 150 |
| XNBR[56] | EG | 9.1wt% | Latex | Nitrogen | 55 | 180 |
| BIIR[57] | GE | 4.0wt% | Solution | Oxygen | 44 | — |
| NRL[58] | rGO | 5.7wt% | Latex | Oxygen | 60 | — |

| | | | | | |
|---|---|---|---|---|---|
| NBR(Present work) | GO 3.0wt% (1.39vol%) | Latex | Nitrogen | 56 | 486 |

## 4.Conclusions

In the work, a facile and green method was developed to prepare GO/NBR nanocomposites for application in gas barrier materials. This method involves the self-assembly of NBR and GO-induced crosslinking process, resulting from generation of radicals by hemolytic bond cleavage at high temperature. In addition, it was found that the GO-induced crosslinking strongly depended on GO content and treated temperature, which were higher than 1.0wt% and 170℃, respectively. The GO-induced crosslinking enhanced effectively interface interaction between GO nanosheets and rubber matrix, meanwhile improved chemical crosslinking density of nanocomposites. A significant enhancement in tensile strength and reduce in gas permeability coefficient of the GO/NBR nanocomposites was obtained to be 145.0% and 56.0% compared to pure NBR, respectively. Moreover, this approach was based on latex mixing and no rubber ingredient was added, indicating environmentally friendly or “green”. Thereby, the work dose not only confirm the formation of GO/NBR nanocomposites with excellent gas barrier property, but also provides a facile and green method to prepare rubber nanocomposites based on GO or rGO for various applications, such as nitrile latex gloves, oil resistant gasket ring, medicine bottle packaging, and so on.

## Acknowledgements

The authors are grateful for the support of the National Natural Science Foundation of China under grants (51773184 and U1810114), Shanxi Provincial Natural Science Foundation of China (201803D421081 and 20181102014), Scientific and Technological Innovation Programs of Higher Education Institutions in Shanxi (2020L0653).

## Conflict of interest

The authors declared that they have no conflicts of interest to this work.

## References

[1] Y.B. Cui, S.I. Kundalwal, S. Kumar, Carbon 98 (2016) 313-333.

[2] J.E. Mark, B. Erman, M. Roand, New York, Academic Press 2013.

[3] J.N. Song, C.B. Chen, Y. Zhang, Compos.Part A-Appl.S. 105 (2018) 1-8.

[4] L. Zheng, S.J errams, T. Su, Z.C. Xu, L.Q. Zhang, L. Liu, S.P. Wen, Composites Part B, 197 (2020) 108186.

[5] K.J. Berean, J.Z. Ou, M. Nour, M.R. Field, M.M. Alsaif, Y.C. Wang, M. Ramanathan, V. Bansal, S. Kentish, C.M. Doherty, A.J. Hill, C. Mcsweeney, R.B. Kaner, K. Kalantar-zadeh, J.Phys. Chem. C 119 (24) (2015) 13700-13712.

[6] Y.R. Liang, W.L. Cao, Z. Li, Y.Q. Wang, Y.P. Wu, L.Q. Zhang, Polym.Test. 27 (3) (2008) 270-276.

[7] O.S. Kwon, D. Lee, S.P. Lee, Y.G. Kang, N.C. Kim, S.H. Song, RSC Adv. 6 (65) (2016) 59970-59975.

[8] Y. Lin, Z.K. Zeng, J.R. Zhu, S. Chen, X. Yuan, L. Liu, RSC Adv. 5 (71) (2015) 57771-57780.

[9] Y.Y. Mao, S.P. Wen, Y.L. Chen, F.Z. Zhang, P. Panine, T.W. Chan, L.Q. Zhang, Y.R. Liang, L. Liu, Sci.Rep. 3 (2013) 2508.

[10] S.K. Kumar, M. Castro, A. Saiter, L. Delbreilh, J.F. Feller, S. Thomas, Y. Grohens, Mater.Lett. 96 (2013) 109-112.

[11] Y. Guan, K.P. Meyers, S.K. Mendon, G.J. Hao, J.R. Douglas, S. Trigwell, S.I. Nazarenko, D.L. Patton, J.W. Rawlins, ACS Appl. Mater. Interfaces 8 (2016) 33210-33220.

[12] S.Q. Yang, H. Wu, C.H. Li, Y. Xiong, S.Y. Guo, ACS Appl. Mater. Interfaces 12 (2020) 3976-3983.

[13] K.S. Novoselov, A.K. Geim, S.V. Morozov, D. Jiang, Y. Zhang, S.V. Dubonos, I.V. Grigorie, A.A. Firsov, Science 306 (5696) (2004) 666-669.

[14] A.K. Geim, K.S. Novoselov, Nat.Mater. 6 (2007) 183-191.

[15] H.L. Kang, K.H. Zuo, Z. Wang, L.Q. Zhang, L. Liu, B.C. Guo, Compos.Sci.Technol. 92 (2014) 1-8.

[16] J.R. Wu, G.S. Huang, H. Li, S.D. Wu, Y.F. Liu, J. Zheng, Polymer 54 (7) (2013) 1930-1937.

[17] G. Scherillo, M. Lavorgna, G.G. Buonocore, Y.H. Zhan, H.S. Xia, G. Mensitieri, L. Ambrosio, ACS Appl. Mater. Interfaces 6 (2014) 2230-2234.

[18] S. Yaragalla, A.P. Meera, N. Kalarikkal, S. Thomas, Ind.Crop. Prod. 74 (2015) 792-802.

[19] B. Ozbas, C.D. O'Neill, R.A. Register, I.A. Aksay, R.K. Prud'homme, D.H. Adamson, Polym.Sci.,Part B: Polym.Phys. 50 (13) (2012) 910-916.

[20] Y.H. Wu, Y. Lin, Y. Wei, S. Chen, S.Q. Liu, L. Liu, Compos.Sci.Technol. 148 (2017) 35-42.

[21] S. Yaragalla, C.S. Chandran, N. Kalarikkal, R.H.Y. Subban, C.H. Chan, S. Tomas, Polym.Eng.Sci. 55 (11) (2015) 2439-2447.

[22] Y. Lin, S.Q. Liu, L. Liu, J.Mater.Chem.C 4 (12) (2016) 2353-2358.

[23] Y.H. Zhan, M. Lavorgna, G. Buonocore, H.S. Xia, J.Mater.Chem. 22 (21) (2012) 10464-10468.

[24] Z.H. Tang, X.H. Wu, B.C. Guo, L.Q. Zhang, D.M. Jia, J.Mater.Chem. 22 (15) (2012) 7492-7501.

[25] L. Zheng, S. Jerrams, Z.C. Xu, L.Q. Zhang, L. Liu, S.P. Wen, Chem.Eng.J. 383 (2020) 123100.

[26] X.L. Hou, J.L. Li, Simon.C. Drew, B. Tang, L. Sun, X.G. Wang, J. Phys. Chem. C 117 (13) (2013) 6788-6793.

[27] R.C. Feng, W. Zhou, G.H. Guan, C.C. Li, D. Zhang, Y.N. Xiao, L.C. Zheng, W.X. Zhu, J. Mater. Chem. 22 (9) (2012) 3982-3989.

[28] L. Valentini, S. Bittolo Bon, M. Hernández, M.A. Lopez-Manchado, N.M. Pugno, Compos.Sci.Technol. 166 (2018) 109-114.

[29] J.A. Mohammad, R. Sheida, R. Katayoon, M. Masoud, A. Fahimeh, RSC Adv. 10 (20) (2020) 11777-11790.

[30] X. Wu, R.W. Field, J.J. Wu, K. Zhang, J.Membrane Sci. 540 (2017) 251-260.

[31] P.J. Flory, J.Chem.Phys. 18 (1950) 108~111.

[32] W.G. Huang, K.H. Wei, C.M. Wu, Polym.Eng.Sci. 44 (11) (2004) 2117-2124.

[33] J.W. Vanderhoff, E.B. Bradford, W.K. Carrington, J. Polymer SCI.: Symposium 41 (1) (1973) 155-174.

[34] L. Konko, S. Guriyanova, V. Boyko, L.C. Sun, D. Liu, B. Reck, Y.F. Men, Langmuir 35 (2019) 6075-6088.

[35] X. Liu, W.Y. Kuang, B.C. Guo, Polymer 56 (2015) 553-562.

[36] Y.H. Zhang, U.R. Cho, Polym.Composite. 39 (9) (2018) 3227-3235.

[37] D. Kuang, L.Y. Xu, L. Liu, W.B. Hu, Y.T. Wu, Appl. Surf. Sci. 273 (2013) 484-490.

[38] A.C. Ferrari, J.C. Meyer, V. Scardaci, C. Casiraghi, M. Lazzeri, F. Mauri, S. Piscanec, D.J iang, K.S. Novoselov, S. Roth, A.K. Geim, Phys. Rev.Lett. 97 (2006) 187401.

[39] M.A. Lopez-Manchado, M. Arroyo, B. Herrero, J. Biagiotti, J. Appl. Polym. Sci. 89 (1) (2003) 1-15.

[40] M. Raef, M. Razzaghi-Kashani, Polymer 182 (2019) 121816.

[41] B. Mensah, K.C. Gupta, G. Kang, Polym.Test. 76 (2019) 127-137.

[42] D.C. Marcano, D.V. Kosynkin, J.M. Berlin, A. Sinitskii, ACS Nano. 4 (2010) 4806-4814.

[43] C.A. Tao, J.F. Wang, S.Q. Qin, Y.N. Lv, Y. Long, H. Zhu, Z.H. Jiang, J. Mater. Chem. 22 (47) (2012) 24856-24861.

[44] W. Gronski, U. Hoffmann, G. Simon, A. Wutzler, E. Straube, Rubb.Chem.Technol. 65 (2) (1992) 63-77.

[45] W. Kuhn, I. Theis, E. Koeller, Mater.Res.Soc. Symp.Proc. 33 (1) (1991) 217-223.

[46] S. Prager, F.A. Long, J.Am.Chem Soc. 73 (1951) 4072-4075.

[47] G.J.V. Amerongen, Rubb.Chem.Technol. 37 (5) (1964) 1065 -1152 .

[48] A.R. PAYNE, J. Appl. Polym. Sci. 6 (19) (1962) 57-63.

[49] J. Fröhlich, W. Niedermeier, H.D. Luginsland, Composites Part A, Appl. Sci. Manu. 4 (36) (2005) 449-460.

[50] M.R. Piggott, Springer Science＆ Business,Media, 2002.

[51] J. Sarabadani, A. Naji, R. Asgari, R. Podgornik, Phys.Rev.B 84 (2011) 155407.

[52] S. Bhattacharyya, C. Sinturel, O. Bahloul, M.L. Saboungi, S. Thomas, J.P. Salvetat, Carbon 46 (7) (2008) 1037-1045.

[53] K.H. Liao, S. Kobayashi, H. Kim, A.A. Abdala, C.W. Macosko, Macromolecules 47 (21) (2014) 7674-7676.

[54] R.K. Bharadwaj, Macromolecules 34 (2001) 9189-9192.

[55] Y.N. Quan, M. Lu, M. Tian, S.K. Yan, Z.Z. Yu, L.Q. Zhang, J. Appl. Polym. Sci. 130 (1) (2013) 680-686.

[56] J. Yang, L.Q. Zhang, J.H. Shi, Y.N. Quan, L.L. Wang, M. Tian, J. Appl. Polym. Sci. 116 (5) (2010) 2706-2713.

[57] M. Kotal, S.S. Banerjee, A.K. Bhowmick, Polymer 82 (15) (2016) 121-132.

[58] N. Yan, G. Buonocore, M. Lavorgna, S. Kaciulis, S.K. Balijepalli, Y.H. Zhan, H.S. Xia, L. Ambrosio, Compos. Sci.Technol. 102 (2014) 74-81.

[59] Z. Zhang, X.R. He, X. Wang, A.M. Rodrigues, R. Zhang, J. Appl. Polym. Sci. 135 (14) (2018) 46091.

[60] Y.H. Zhang, U.R. Cho, Polym. Composite. 39 (9) (2018) 3227-3235.

[61] Y.Q. Wang, Y.P. Wu, H.F. Zhang, L.Q. Zhang, B. Wang, Z.F. Wang, Macromol. Rapid Commun. 25 (23) (2004) 1973-1978.